BMC Cancer

https://doi.org/10.1186/s12885-026-16310-w

Article in Press

NAV-005, a high-affinity MUC16/CA125 antagonist for the treatment of humoral immunosuppressed cancers

Received: 12 November 2024

Accepted: 3 June 2026

Published online: 20 June 2026

Cite this article as: Nicolaides N.C., Kline J.B. & Grasso L. NAV-005, a high-affinity MUC16/CA125 antagonist for the treatment of humoral immunosuppressed cancers. *BMC Cancer* (2026). https://doi.org/10.1186/s12885-026-16310-w

Nicholas C. Nicolaides, James Bradford Kline & Luigi Grasso

NAV-005, a high-affinity MUC16/CA125 antagonist for the treatment of humoral immunosuppressed cancers

Nicholas C. Nicolaides*, James Bradford Kline and Luigi Grasso

Navrogen Inc. 1837 University Circle, Cheyney, PA 19319

*Correspondence to: Nicholas C. Nicolaides Email: nick@navrogen.com

Running title: CA125 antagonists for treating immunosuppressed cancers

Abstract

Objective This study aimed to develop a high-affinity therapeutic antagonist to overcome tumor-produced MUC16/CA125 (herein CA125) mediated immunosuppression of anticancer therapeutic antibodies and antibody-drug conjugates (ADCs). The goal was to generate an antagonist that blocks CA125 binding to IgG1 antibodies, restores antibody interaction with CD16a Fc-γ-activating receptors (herein CD16a) and C1q protein, and re-enables maximal antibody-dependent cellular cytotoxicity (ADCC) and complement-dependent cytotoxicity (CDC) against cancer cells. Since CA125 binding to ADCs impairs its cytotoxicity by reducing ADC internalization, the antagonist was further designed to restore maximal ADC activity. Achieving these aims supports the clinical development of CA125 antagonists for treating cancers marked by humoral immunosuppression.

Methods Human IgG1 Fc fusion proteins with varying mesothelin binding domain (MBD) motifs were engineered and tested for high-affinity CA125 binding. Antagonist efficacy was assessed by measuring restoration of CD16a and C1q binding to IgG1 antibodies suppressed by CA125. ADC internalization assays evaluated the effect of CA125 and antagonists on ADC uptake. Cellular assays, including Jurkat-CD16a reporter and PBMC-based ADCC assays,

measured restoration of antibody-CD16a mediated immune effector cell killing of target cells. Cytotoxicity assays assessed CDC and ADC mediated cell killing.

Results NAV-005 (MBD2-Fc), a lead antagonist, bound CA125 with high affinity and blocked its binding to IgG1-type antibodies. NAV-005 reversed CA125-induced antibody immunosuppression, thereby restoring IgG1 mediated ADCC and CDC by preventing CA125-IgG1 interaction. NAV-005 also prevented CA125-ADC cell surface interactions, thereby restoring maximal ADC internalization and target cell killing.

Conclusion Tumor-produced CA125 impairs therapeutic antibody and ADC efficacy via humoral immunosuppression. NAV-005 counteracts this effect, restoring antitumor activity of antibodies and ADCs in CA125-expressing cancers. These results support the continued development of CA125 antagonists as adjuncts to antibody-based cancer therapies.

Keywords: CA125, humoral immunosuppression, humoral immuno-oncology (HIO), antibody dependent cellular cytotoxicity (ADCC), CD16a Fc receptor, complement dependent cytotoxicity (CDC), C1q protein, antibody-drug conjugate (ADC), ADC internalization, cancer therapy

Introduction

MUC16/CA125 is a high molecular weight glycoprotein overexpressed in various carcinomas and follicular lymphomas (1,2). CA125 exists in both soluble and membrane-bound forms. In oncology, CA125 is routinely monitored using regulatory agency-approved serum diagnostics (3,4). While a serum concentration exceeding 35 U/mL signals tumor presence in recurrent disease, the local concentration at the tumor site can be 100 to 2,000 times higher than in patient serum (5,6). The serum half-life of CA125 is approximately six days, and its high production rate

(~2.5 pg/cell/day) likely accounts for its significant accumulation in both the tumor microenvironment and serum (7,8). In either form, CA125 has been shown to suppress humoral immune responses by directly binding to the CDR3-FW4 heavy chain region in a subset of IgG1-type antibodies, which in turn allosterically alters the Fc region. This results in reduced engagement with the CD16a Fc-γ-activating receptor (FcγRIII) and the complement-initiating C1q protein, a process known as Humoral Immuno-Oncology (HIO) (9). Recent studies indicate that tumors use HIO factors to suppress humoral immune pathways, leading to diminished antibody-mediated cytotoxicity via antibody-dependent cellular cytotoxicity (ADCC) and complement-dependent cytotoxicity (CDC) mechanisms (10-13). Several regulatory agency-approved IgG1-type antibodies, such as rituximab, alemtuzumab, trastuzumab, pertuzumab, cetuximab, and daratumumab, as well as numerous experimental anticancer antibodies, rely on humoral immune mechanisms for target cell killing (9,14-21). Humoral immune activation also occurs naturally in patients with indolent disease, dysregulated cells, and in response to vaccines (22-24). However, although cancer patients generate autoantibodies to tumor-associated antigens, these antibodies often fail to limit tumor growth, possibly due to low titers, low affinity, or humoral immunosuppression (13). These findings highlight the need for tools and therapeutic agents capable of detecting and overcoming humoral immunosuppression mediated by HIO factors, such as CA125, and other immunosuppressive proteins. One approach to address this need is to develop high affinity antagonists that can bind HIO factors and potentially alter their binding activity on humoral immune components, including the tumor targeting antibody itself. Previous studies have reported that a region of the mesothelin (MSLN) protein can bind CA125 with high affinity (25,26), suggesting its potential utility in altering CA125 binding to

IgG1. The focus of this study was to evaluate the potential of MSLN-based antagonists to address the unmet need to treat immunosuppressed CA125-positive cancers.

Experimental methods

Cell lines HEK293-F (purchased from Thermo Fisher Scientific), OVCAR3 ($CA125^+/MSLN^+/FRA^+/HER2^+$) (purchased from ATCC), OVCAR-KD1 ($CA125^-/MSLN^+/FRA^+/HER2^+$) (derived from OVCAR3), OVCAR-CD20 (derived from OVCAR3 and engineered to express cell surface human CD20), Jurkat-CD16a luciferase (purchased from Promega), Daudi (purchased from ATCC), SW1990 (purchased from ATCC) and YOU-meso (obtained from Dr. Raffit Hassan) were all grown in RPMI 1640 supplemented with 2 mM L-glutamine, 100 U/mL penicillin/streptomycin, and 7.5% (v/v) fetal bovine serum (R7.5). OVCAR-KD1 cells were grown in R7.5 containing 1.5 μg/mL puromycin to retain CA125 shRNA suppression. OVCAR-CD20 cells were grown in R7.5 media supplemented with 30 μg/mL blasticidin selection to retain CD20 expression. Jurkat-CD16a luciferase cells were grown in R7.5 media supplemented with 25 μg/mL G418 and 10 μg/mL hygromycin to retain expression of reporter gene elements. HEK293-MDB-Fc cells were maintained in BalanCD media supplemented with 100 μg/mL zeocin to retain MDB-Fc expression. Expression of key antigens mesothelin (MSLN), CD20, folate receptor alpha (FRA), human epidermal growth factor receptor 2 (HER2) and CA125 were confirmed by immunoblot of lysates from each cell line (SFigure 1).

Antibodies SS1 is an anti-MSLN antibody purchased from MedChem and is also referred to as MORAb-009 and amatuximab (33-35). Rituximab (RTX) is an anti-CD20 purchased from MedChem (9). Pertuzumab (PTZ) is an anti-HER2 antibody purchased from MedChem (18). NAV-007 is an anti-FRA antibody developed at Navrogen.

Generation of MDB-Fc fusion proteins The generation of stable MSLN binding domain-Fc (MBD-Fc) fusion-producing cell lines were created using a pCMV-based bicistronic expression vector as previously described (9). cDNAs encoding MBD-Fc fusion proteins were synthesized and cloned between the CMV promoter and the IRES-zeocin resistance gene cassette. In the MBD1-Fc construct (contains one MBD), 64 amino acids corresponding to residues 239-302 of the human MBD sequence (GenBank: KAI2576270.1) were fused to residues 99-330 of the human IgG1 heavy chain domains CH2-CH3 (GenBank: AXN93646.1). In MBD2-Fc (contains two MBDs) and MBD3-Fc (contains three MBDs), two or three 64-aa MBD encoding fragments were added, respectively, each separated by a GGGGS encoding spacer fragment. The IgG1 domain component has a 683 nM binding affinity to the dominant phenylalanine (aa158) CD16a allotype (CD16a-158F) (12). All constructs were sequenced to ensure proper cDNA integrity. Recombinant expression plasmids were transfected into FreeStyle™ HEK293-F cells to produce stable MBD-Fc fusion protein producing cell lines. Briefly, 0.5×10^6/mL cells were seeded in serum-free HEK293 BalanCD medium (Irvine Scientific) supplemented with 2 mM glutamine, 100 U/mL penicillin, and 100 µg/mL streptomycin in a T25 vented flask and grown on a shaker platform at 130 RPM at 37°C with 5% CO_2. The next day, transfections were performed using 2 µg of each plasmid DNA in 0.2 mL of OptiPRO™ SFM (Thermo Fisher Scientific) with 15 µL of polyethyleneimine Max Mw 40,000 (Polysciences). Plasmid mixtures were incubated for 30 minutes then added to the cells. Cultures were grown as above for 48 hours then plated in 10 cm dishes in RPMI 1640 (Caisson Labs) containing 2 mM glutamine, 100 U/mL penicillin, 100 µg/mL streptomycin, 7.5% (v/v) fetal bovine serum and 200 µg/mL zeocin (Thermo Fisher Scientific) for 10 days. After selection, cells were subcloned by limiting dilution, and their conditioned media were tested for MBD-Fc protein expression by ELISA using an anti-human

IgG1-HRP antibody as probe. Positive subclones were expanded in serum-free HEK293 BalanCD medium supplemented with 2 mM glutamine, 100 U/mL penicillin, 100 µg/mL streptomycin, and 200 µg/mL zeocin. Cultures were grown to confluence, conditioned media were harvested and proteins were purified via protein A column affinity chromatography (Amshpere) using the IgG Binding/Gentle Elution (pH 6.6) buffer system (Thermo Scientific). Eluted samples were dialyzed at 4ºC in Dulbecco's PBS Ca^{--}/Mg^{--} ($DPBS^{-/-}$) buffer using Snakeskin dialysis tubing (MWCO 10,000) (Thermo Scientific). Stable clones were determined as those producing single fusion species visualized on non-denaturing 4-12% Bis-Tris SDS-PAGE gels in 1X MOPS [0.2M (3-(N-morpholino) propanesulfonic acid, 0.05M NaAC, 0.01M EDTA, pH 7.0] running buffer. Clones producing single species at the predicted molecular weight were banked.

Direct ELISA MBD-Fc/CA125 binding assays 96-well microplates were coated with 5 µg/mL of recombinant N-terminal (CA125-N, amino acids 1-546) and C-terminal (CA125-C, amino acids 13360-14347) CA125 proteins (R&D Systems), 30 KU/mL full length CA125 (Lee Biosolutions) or 5 µg/mL human serum albumin (HSA), used as a negative control, in 50 mM carbonate buffer, pH 9.5, overnight at 4°C. Microplates were subsequently washed with 50 mM phosphate buffer, pH 7.2 (PB), and blocked for 1 hour at room temperature in PB plus 5% (w/v) BSA (PB-5). MBD-Fc fusion proteins were biotinylated via the EZ-Link Sulfo-NHS-Biotin Kit (Thermo Scientific) and used as probes. Triplicate wells were probed with 2.5 µg/mL biotinylated MBD-Fc proteins in PB plus 0.5% (w/v) BSA (PB-0.5). Plates were then washed with PB and probed with 300 ng/mL streptavidin-HRP (Jackson Labs) in PB-0.5 for 1 hour. After washing with PB, TMB colorimetric substrate (Thermo Fisher Scientific) was added for 5 minutes at room temperature, followed by the addition of an equal volume of 0.1 N H_2SO_4 stop

buffer. Binding was quantified by measuring the absorbance at 450 nm on a Varioskan plate reader (Thermo Fisher Scientific). All assays were run in triplicate. Statistical significance was determined via Student's t test comparing CA125 binding to HSA negative control.

CD16a and C1q binding assays 96-well microplates were coated with 2.5 μg/mL RTX in 50 mM carbonate, pH 9.5, overnight at 4°C. Plates were washed with PB and blocked for 1 hour at room temperature in PB-5. CD16a (Sino Biologicals) and C1q (Pierce) proteins were biotinylated via the EZ-Link Sulfo-NHS-Biotin Kit (Thermo Scientific) and used as probes. Next, wells were washed with PB and probed with 2.5 μg/mL biotinylated CD16a or 1 μg/mL C1q protein with or without 20 μg/mL MBD-Fc fusion proteins +/- 30 KU/mL CA125 in PB-0.5 for 1 hour at room temperature. The plates were subsequently washed with PB and probed with 300 ng/mL streptavidin-HRP in PB-0.5. After washing with PB, TMB colorimetric substrate was added for 5 minutes at room temperature, followed by the addition of an equal volume of 0.1 N H_2SO_4 stop buffer. Binding was quantified by measuring the absorbance at 450 nm on a Varioskan plate reader. Experiments were run in multiple triplicate assays. Statistical significance was determined via ANOVA comparing CA125 treated to no treated wells.

MBD-Fc binding affinity to CA125 via surface plasmon resonance (SPR) Biacore T200 (GE Healthcare) was employed to determine the binding affinities of MBD1-Fc and MBD2-Fc to CA125. MBD-Fc proteins were captured on a Series S Sensor Protein A chip in HBS-EP buffer (10 mM HEPES, 150 mM NaCl, 3 mM EDTA, 0.05% Tween-20, pH 7.4). Next, various concentrations of recombinant C-terminal CA125 were injected at a flow rate of 30 μL/minute to determine the association constants, and the flow cells were subsequently washed to determine the dissociation constants to obtain the overall binding affinity (K_D) via Biacore T200 Evaluation software version 3.1.

Jurkat-CD16a-luciferase ADCC reporter assays The Jurkat-CD16a-luciferase (Jurkat-CD16a) ADCC reporter cell assay (Promega) was used to test the effects of CA125 and MBD-Fc on CD16a activation as previously described (11). To determine the effects of CA125 and MBD-Fc on receptor activation, OVCAR3 cells were diluted to 5×10^4 cells/mL in ADCC assay buffer (RPMI + 2mM L-glutamine + 1% (v/v) low-Ig FBS), and 0.1 mLs of cells were seeded in black 96-well microplates in triplicate. The next day, 2.5 μg/mL of the anti-FRA NAV-007 antibody (Navrogen unpublished reagent) was added along with 100,000 Jurkat-CD16a cells +/- 30 KU/mL CA125, +/- 20 μg/mL MBD-Fc proteins simultaneously in a mixing tube, and cell mixture was then added to each corresponding well. Plates were incubated overnight at 37°C in 5% CO_2. Reporter cell activation was detected via Bio-Glo™ (Promega) luciferase substrate following the manufacturer's protocol, and lumens were quantified on a Varioskan plate reader. The percentage of Jurkat-CD16a stimulation was calculated by the formula ((NAV-007+CA125+MBD-Fc lumens / NAV-007+CA125 lumens)-1) × 100. Experiments were run in multiple triplicate assays. Statistical significance was determined via ANOVA comparing antibody plus CA125 alone vs MBD-Fc treated wells.

CDC assays Daudi target cells were seeded at 25,000 cells/well in black 96-well microplates in RPMI containing 1% (v/v) FBS, 2.5 μg/mL rituximab (RTX) antibody, and 10% (v/v) rabbit complement (Bio-Rad), with or without 30 KU/mL CA125 or 20 μg/mL MBD-Fc proteins in triplicate. The plates were incubated at 37°C in 5% CO_2 for 2 hours. After incubation, Cell Titer-Glo® solution was added to the wells, and the samples were processed according to the manufacturer's protocol (Promega). The percentage of CDC was calculated by the formula (1-(RTX+CA125+MBD-Fc+complement lumens / RTX+CA125+complement lumens)) × 100.

Experiments were run in multiple triplicate assays. Statistical significance was determined via ANOVA comparing antibody plus CA125 alone vs MBD-Fc treated wells.

PBMC ADCC assays Primary human peripheral blood cells (PBMCs) obtained from a commercial vendor (BioIVT) were used to test the effects of membrane-bound CA125 and MBD-Fc on ADCC. Briefly, 5,000 OVCAR-CD20 ($CA125^+/HER2^+/CD20^+$) cells were plated in black 96-well microplates. The next day, wells were washed with $DPBS^{-/-}$ and seeded with 100,000 PBMCs/well in ADCC assay buffer (RPMI + 2 mM L-glutamine + 1% (v/v) low-Ig FBS) supplemented with 2.5 μg/ml RTX, pertuzumab (PTZ), and/or 20 μg/mL MDB1-Fc or MDB2-Fc in triplicate. To determine the effect of endogenous CA125 produced from OVCAR-CD20 cells on ADCC, 2.5 μg/mL of RTX or PTZ were incubated +/- 20 μg/mL MBD-Fc proteins in triplicate. The plates were incubated for 16 hours at 37°C in 5% CO_2 then washed, and the viability of the adherent OVCAR-CD20 cells was analyzed via Cell Titer-Glo® (Promega) luciferase substrate and lumens quantified via a Varioskan plate reader. The percent ADCC was calculated as (1-(Ab+PBMC lumens / PBMC lumens)) × 100. Enhanced ADCC activation was calculated as 1-(Ab+MBD-Fc+PBMC lumens / Ab+PBMC lumens). Experiments were run in multiple triplicate assays. Statistical significance was determined via ANOVA comparing % ADCC of antibodies or MBD-Fc proteins to untreated wells or antibodies plus MBD-Fc to untreated wells.

Generation of antibody-drug conjugates (ADCs) and target cell killing assays The SS1-SN38 ADC was generated via the reduced interchain Cys–maleimide method (27, 28) and the cleavable linker-toxin Azide-PEG4-Val-Cit-PAB-SN38. Briefly, the SS1 antibody was partially denatured via TCEP at the optimal incubation time at 37°C and then cooled on ice. Next, SN38-linker toxin (Levena Biopharma) was added to the denatured antibody and incubated at room temperature for 1 hour. The reactions were then desalted using Zeba columns (Thermo Fisher Scientific), and the buffer was exchanged with $DPBS^{-/-}$. The drug-to-antibody ratio (DAR) was determined via hydrophobic interaction chromatography to be 3.5. To test for ADC killing of target cells, clear 96-well microplates were seeded with 5,000 parental OVCAR3, isogenic OVCAR-KD1, SW1990 (25) and YOU-meso (26) cells/well and grown overnight at 37°C in 5% CO_2. The next day, the plates were washed with DPBS $^{-/-}$, and 100 ng/mL of SS1-SN38 +/- 20 μg/mL MBD2-Fc, 20 μg/mL MBD2-Fc only, 2.3 nM SN38 or media only were added to the cells in triplicate, and the plates were incubated for 96 hours at 37°C in 5% CO_2. Wells were then washed in $DPBS^{-/-}$ and quantified via crystal violet staining as previously described (27). Crystal violet-stained wells were solubilized with 1% (w/v) SDS and quantified on a Varioskan plate reader at 570 nm. The percentage of ADC killing was calculated by the formula (1-(treated cells / untreated cells)) × 100. Significance was determined via Student's t test. The IC_{50} (ng/mL) for SS1-ADC against each cell line is listed in each column in red. These were calculated from a titration of SS1-ADC against each cell line and calculated using the formula above and GraphPad Prism Ver. 8.0.2 (GraphPad Software, Inc.).

Antibody internalization assays The pHrodo™ Red Avidin internalization assay (Invitrogen) was employed to monitor the cellular internalization of antibodies +/- MBD2-Fc over a time course. Biotinylated RTX and SS1 antibodies were used to generate pHrodo-labeled probes following the manufacturer's protocol. Briefly, equimolar amounts of biotinylated antibody and pHrodo Red reagents were added to RPMI plus 1% (w/v) BSA for 1 hour on ice. After incubation, the mixtures were centrifuged for 5 minutes at 12,000 × g to remove the aggregates, and the supernatants were collected and quantified via Nanodrop (Thermo Fisher Scientific).

To prepare the cells for pHrodo internalization analysis, black 96-well microplates were seeded with $1x10^5$ OVCAR3 and OVCAR-KD1 cells and grown overnight at 37°C in 5% CO_2 to allow the cells to adhere to the well surface. The next day, the plates were incubated on ice for 1 hour, washed with ice cold $DPBS^{-/-}$ and incubated with 10 μg/mL of each pHrodo-antibody +/- 10 μg/mL MBD2-Fc suspended in ice-cold RPMI plus 1% (w/v) BSA in triplicate. Plates were read for internalization by measuring pHrodo pH-sensitive dye fluorescence at 566/590 nm excitation/emission at various timepoints ranging from 1 minute to 24 hours of incubation at 37°C in 5% CO_2 via a Varioskan plate reader. The percent internalization was calculated as the relative fluorescence unit (RFU) at each timepoint (TX)/fluorescence at T0. Enhanced internalization was determined in OVCAR3 by comparing SS1 internalization alone with those treated with antibody plus MBD2-Fc. OVCAR-KD1 was used to monitor SS1 uptake +/- MBD-Fc vs OVCAR3. RTX was used as a negative control as neither cell line expresses CD20 antigen. Statistical significance was determined via Student's t test.

Statistics Statistical significance was determined via paired two-sided Student's t test or one-way ANOVA using GraphPad Prism Ver. 8.0.2 software as indicated for each set of

experiments. Values are represented as * $P < 0.05$, ** $P < 0.01$, *** $P < 0.001$, **** $P < 0.0001$.

Results

To develop a CA125 antagonist capable of overcoming the humoral immunosuppression of therapeutic antibodies in patients with CA125-positive cancers, we engineered a construct similar to HN125 (26). This construct, termed MBD1-Fc, consists of a human IgG1 Fc domain containing the hinge region fused to the minimal MSLN CA125 binding domain (MBD). We first evaluated the ability of MBD1-Fc to bind both the intact CA125 protein and its recombinant C-terminal domain (CA125-C), the region to which MSLN is known to bind (29). As demonstrated in Figure 1A, MBD1-Fc bound to both intact CA125 and CA125-C, but not to the recombinant CA125-N domain. CA125 mediates its immunosuppressive effect by directly binding the IgG1 heavy chain variable domain (9), thereby reducing the capacity of IgG1 antibodies to engage with the CD16a Fc-γ-receptor (hereafter CD16a) or the C1q protein as a result of allosteric changes within the Fc domain (11-13). The suppressive effect of CA125 on antibody-CD16a binding is illustrated in Figure 1B, where CA125 significantly inhibited RTX-CD16a binding (bar 2). However, addition of MBD1-Fc did not prevent CA125-mediated inhibition of antibody-CD16a binding (bar 4). These findings suggest that MBD1-Fc binding was either insufficient to disrupt the CA125-antibody interaction or that the interaction motif remained unaffected by MBD1-Fc binding at the concentrations tested.

To address the potential limitations of suboptimal MBD1-Fc binding, we hypothesized that IgG1 fusions containing two or more MBD motifs could enhance the avidity of the fusion protein and potentially overcome CA125-mediated suppression. To test this, we generated MBD-Fc fusion proteins with two (MBD2-Fc) and three (MBD3-Fc) MBD motifs, each separated by a GGGGS

amino acid spacer (highlighted in red, Figure 2A). These fusion proteins were constructed using expression plasmids similar to those for MBD1-Fc and formed single-species homodimers, attributable to the maintained hinge region in the Fc portion (Figure 5C). All three MBD-Fc fusion proteins were evaluated in CA125 binding assays. As illustrated in Figure 2B, all MBD-Fc proteins bound CA125 significantly more than the HSA negative control ($P < 0.001$), with MBD2-Fc and MBD3-Fc exhibiting stronger binding than MBD1-Fc, likely due to increased avidity from multiple MBD motifs. We next assessed whether these fusion proteins could overcome CA125-mediated inhibition of antibody-CD16a binding via ELISA. Figure 2C shows that both MBD2-Fc and MBD3-Fc restored antibody-CD16a binding in the presence of CA125, whereas MBD1-Fc did not ($P < 0.0001$). A similar effect was observed for antibody-C1q binding (Figure 2D). Importantly, no significant differences were found between MBD2-Fc and MBD3-Fc in CA125 binding ($P > 0.05$), nor was there additional improvement in overcoming CA125-mediated suppression of CD16a or C1q binding to antibodies ($P > 0.05$), indicating that two MBD motifs are sufficient for maximal CA125 antagonism.

Given that fusion proteins with multiple MBD motifs demonstrated greater activity than those with a single motif, we next analyzed their binding affinities for CA125. Since MBD2-Fc and MBD3-Fc showed similar values in CA125 binding and competition ELISAs (Figure 2), we only compared the binding affinities of MBD1-Fc and MBD2-Fc using surface plasmon resonance (SPR). As shown in Figure 3, MBD2-Fc exhibited a 4.3-fold higher binding affinity than MBD1-Fc (15 pM vs 65 pM, respectively). Although no prior reports have established such a threshold, these findings suggest that a minimum binding affinity may be necessary for a CA125 antagonist to effectively counteract the immunosuppressive effects of CA125 on IgG1-type antibody immune effector functions.

To investigate whether the molecular effects of MBD2-Fc translated into functional responses, we tested MBD1-Fc and MBD2-Fc in ADCC and CDC assays. For ADCC analysis, we employed the Jurkat-CD16a ADCC reporter assay, which measures CD16a activation as a surrogate for ADCC, as described in the experimental methods as well as standard ADCC assays using primary PBMC immune effector cells. Briefly, FRA-expressing OVCAR3 cells were plated into black 96-well microplates and treated the next day with the anti-FRA NAV-007 humanized IgG1 antibody +/- CA125 and +/- MBD-Fc fusion proteins or MBD-Fc fusion proteins alone. Assays were run for 16 hours and then analyzed for CD16a activation. NAV-007 activation of Jurkat-CD16a cells exposed to CA125 was significantly improved by 70% ($P < 0.0001$) in the presence of MBD2-Fc, whereas no improvement was observed when MBD1-Fc was used (Figure 4A). These results are consistent with the CA125 binding and CA125 competition data shown in Figure 2B and 2C. The MBD-Fc fusion proteins alone had no receptor activation, which is consistent with other assays conducted within this study. CDC analysis using CD20-positive Daudi cells and the anti-CD20 RTX antibody showed similar effects to those of MBD2-Fc on Jurkat-CD16a stimulation in the presence of CA125. As shown in Figure 4B, compared with MBD1-Fc and antibody alone, MBD2-Fc significantly increased the CDC activity of RTX against Daudi target cells in the presence of CA125 by 40% ($P < 0.0001$). These results are consistent with the CA125 binding and CA125 competition data shown in Figure 2A and 2D. Moreover, these data are consistent with previous findings that CA125 can bind to IgG1-type antibodies and allosterically alter its Fc domain, thereby reducing the ability of CD16a and C1q to engage the antibody and elicit downstream immune effector activity (9). The inhibition of CA125 binding to IgG1 removes this allosteric effect on the antibody.

Given that membrane-bound CA125 on the cell surface has been shown to suppress IgG1-type antibody-mediated ADCC and CDC activity (9-13), we investigated the effect of MBD-Fc fusion proteins on enhancing ADCC against CA125-expressing target cells. We used the OVCAR-CD20 cell line, which naturally expresses HER2 and has been engineered to express CD20 (SFigure 1). Cells were plated in black 96-well microplates and treated the next day with either anti-HER2 PTZ or anti-CD20 RTX antibodies, along with human PBMC immune effector cells. After overnight incubation, target cell viability was assessed. Because MBD-Fc fusion proteins can bind membrane-bound CA125 on OVCAR-CD20 cells and may exert cytotoxic effects (26), they were tested alone and in combination with antibodies and PBMCs. As shown in Figure 5A, neither MBD1-Fc nor MBD2-Fc induced target cell killing, in contrast to RTX and PTZ ($P < 0.0001$), indicating that MBD-Fc proteins cannot elicit ADCC independently. However, MBD2-Fc, but not MBD1-Fc, significantly enhanced ADCC activity of both RTX (56.4%) and PTZ (58.4%) ($P < 0.0001$) (Figure 5B). This enhancement likely results from MBD2-Fc blocking CA125-antibody interactions on the OVCAR-CD20 cell surface, thereby maximizing antibody-CD16a engagement and subsequent immune effector cell cytotoxicity. These findings are consistent with the molecular data in Figure 2C. To confirm equivalent amounts of MBD-Fc proteins were used, 500 ng of each was analyzed by non-denaturing SDS-PAGE, demonstrating similar concentration and homogeneity (Figure 5C).

Previous studies have demonstrated that membrane-bound CA125 on the cell surface can impair ADC cytotoxicity against target cells (27), primarily by reducing cellular internalization required for optimal ADC activity (30-32). To assess whether MBD2-Fc can improve ADC cytotoxicity, we utilized the anti-MSLN SS1 antibody, which is known to be immunosuppressed by CA125 (27,35). We generated an SS1-SN38 ADC by conjugating the SN38 topoisomerase I inhibitor to

SS1 via a PEG4 valine-citrulline cleavable linker. We compared the effects of membrane-bound CA125 on ADCs by examining the cytotoxicity of SS1-SN38 ADC in the $MSLN^+/CA125^+$ ovarian cancer cell line OVCAR3 and its isogenic OVCAR3-KD1 cell line, in which CA125 expression is significantly reduced via shRNA (SFigure 1) (11,27,35). As shown in Figure 6, OVCAR-KD1 cells were significantly more sensitive to SS1-SN38 ADC-mediated killing than parental OVCAR3 cells ($P < 0.01$). This greater sensitivity is likely due to the absence of CA125, which otherwise binds to the ADC on the cell surface and slows its internalization, thereby limiting internal payload liberation and cytotoxicity (30,32). This is reflected in the SS1-SN38 ADC IC_{50}, where OVCAR-KD1 cells are 2.7-fold more sensitive than OVCAR3 parental cells, likely due to reduced CA125-SS1 ADC interaction at the OVCAR3 cell surface. Notably, addition of MBD2-Fc to SS1-SN38 ADC increased cytotoxicity against OVCAR3 parental cells to levels comparable to the OVCAR-KD1 line (86% vs. 87% cytotoxicity, respectively; $P < 0.01$). Enhanced SS1-SN38 ADC cytotoxicity by MBD2-Fc was also observed in other $CA125^+/MSLN^+$ cancer cell lines (SFigure 1A), including SW1990 pancreatic cancer and YOU-meso mesothelioma cell lines ($P < 0.004$), which showed similar IC_{50} values (102.8 and 92.6 ng/mL, respectively) to the OVCAR3 parental line (93.6 ng/mL). Free SN38 served as a positive control at its predetermined EC_{90} of 2.3 nM, yielding consistent maximal cytotoxicity across all cell lines (79.6% ± 1.8%). As expected, MBD2-Fc alone did not affect target cell cytotoxicity. These results correlate with increased ADC internalization, as shown in Figure 7A whereby SS1 uptake by OVCAR-KD1 cells was 30% greater than by parental OVCAR3, and adding MBD2-Fc to SS1-treated OVCAR3 cells resulted in a 20% increase in SS1 uptake compared to OVCAR3 alone ($P < 0.01$). These findings align with previous reports linking ADC cytotoxicity to internalization rates (27,30-32). A schematic overview of this mechanism is illustrated in

Figure 7B, showing that MBD2-Fc (NAV-005) enhances ADC uptake by liberating ADC bound to membrane CA125. This is further supported by the observation that SS1 alone in OVCAR-KD1 and SS1 + MBD2-Fc in OVCAR3 cells have similar internalization rates vs. SS1 alone in OVCAR3, while the addition of MBD2-Fc to SS1 does not enhance SS1 internalization in OVCAR-KD1 cells ($P > 0.05$; Figure 7A).

Discussion

Strategies to overcome humoral immunosuppression caused by HIO factors are rapidly evolving within the pharmaceutical industry. These strategies include screening for antibodies that may be vulnerable to humoral immunosuppression by cancers expressing specific HIO factors, followed by either avoiding their use in HIO-positive patients or engineering HIO-refractory antibodies, as previously described (9,31). Although avoiding HIO-positive patients when administering HIO-susceptible antibody-based therapies may be prudent, the diminished efficacy of certain regulatory agency-approved targeted therapies due to humoral immunosuppression remains a significant unmet medical need. Employing HIO factor antagonists, such as MBD2-Fc (NAV-005), in combination with antibody-based standard-of-care therapies for CA125-expressing cancers may offer a promising solution to this challenge. Here, we present experimental evidence supporting the use of HIO factor antagonists as a viable strategy to address this issue.

While Xiang et al. (26) reported that their CA125-binding Fc fusion protein HN125 elicits ADCC activity on cancer cells expressing membrane-bound CA125, we were unable to replicate these findings. Neither MBD1-Fc nor MBD2-Fc mediated ADCC killing in the absence of a targeting antibody (Figure 5A). ELISA analysis demonstrated that both MBD1-Fc and MBD2-Fc bind the CD16a receptor at levels comparable to the RTX antibody ($P < 0.001$), thereby excluding ineffective CD16a engagement as the cause for the lack of ADCC activity (SFigure 2).

The observed differences between HN125 and MBD-Fc proteins may be attributed to construct design. The HN125 Fc domain comprises IgG1 wild-type sequences from residues 104 to 330, whereas the NAV-005 Fc domain includes residues 99 to 330. This five-amino-acid difference could affect the positioning and dynamic structure of HN125, potentially making it more conducive to CD16a engagement in a stimulatory manner, as previously reported for antibodies (36,37). Alternatively, differences in ADCC activity might result from varying experimental conditions or from the CD16a allotype in the effector cells used (12,36,37). Our ADCC assays utilized a PBMC effector-to-target cell ratio of 20:1, while Xiang et al. used a much higher ratio of 100:1. These elevated ratios could explain the measurable ADCC elicited by HN125. Additionally, the PBMCs in our studies were heterogeneous for low (CD16a-158F) and high (CD16a-158V) affinity CD16a (12), whereas Xiang et al.'s effector cells may have been homozygous for the high-affinity receptor, potentially enabling stronger engagement with target cell-bound HN125, a well-documented factor in ADCC responses (12,36,37).

Surface plasmon resonance analyses (Figure 3) have provided valuable insight into why MBD2-Fc (NAV-005) may outperform MBD1-Fc as an antagonist. Although both proteins exhibit similar association constants, MBD2-Fc has a dissociation constant that is 4.6-fold lower than that of MBD1-Fc, enabling it to more effectively block CA125 binding to antibodies. Furthermore, Rupert et al. (38) demonstrated that MSLN binds to the extracellular C-terminus of CA125 within the SEA repeat domain, which contains 16 repeats with minor amino acid variations. Their analysis revealed that MSLN can bind all repeats with varying affinities, with the highest affinity for SEA10 (K_D = 900 nM). The 4.3-fold increased binding affinity of MBD2-Fc may facilitate more stable attachment to SEA10 and improved interaction with lower-affinity

repeats compared to MBD1-Fc, resulting in enhanced inhibition of CA125-antibody binding via increased avidity within the SEA repeat region.

CA125 is expressed in several cancers for which antibody-based therapeutics are approved, such as follicular lymphoma, ovarian, breast, and colorectal cancers (39-42). Elevated CA125 levels are often associated with poorer clinical outcomes. While direct confirmation requires a translational HIO-focused clinical trial, these associations may stem from the negative impact of HIO factors like CA125 on the immune effector mechanisms of therapeutic antibodies. Supporting the importance of immune effector function, our group recently demonstrated that NAV-006, a genetically optimized, CA125-refractory RTX with a single amino acid variant that significantly reduces CA125-NAV-006 binding, shows improved efficacy over parental RTX in *in vivo* models of human B-cell lymphoma in the presence of CA125 (43). In addition, MBD2-Fc (NAV-005) has been shown to reverse CA125-mediated suppression of SS1-SN38 ADC (Figure 6), consistent with our previous findings linking CA125 expression to reduced antibody internalization and diminished ADC potency (27). Collectively, these results support further investigation of MBD2-Fc (NAV-005) as a potential enhancer of IgG1-type antibody-based therapies in CA125-expressing cancers. Future studies will include dosing analyses to determine whether co-administration of NAV-005 with antibody or ADC is as effective in enhancing drug response as more frequent dosing of NAV-005, depending on CA125 levels and the pharmacokinetic properties of the fusion protein in animal and human studies. Our preliminary assessment suggests that co-administration may be an optimal strategy to maximize patient compliance and efficacy. NAV-005's mechanism for enhancing antibody and ADC efficacy is best utilized by antagonizing CA125 during peak antibody or ADC exposure (Cmax), which typically occurs within the first two hours post-dose (44). Moreover, because NAV-005 acts

directly on CA125 rather than on the antibody or ADC (11,13,27), it is unlikely to alter the pharmacokinetic or pharmacodynamic properties of the antibody, a profile supportive for co-administered agents (45). These points will be addressed in forthcoming *in vivo* experimental models.

Experimental designs were employed to rigorously assess the reproducibility of findings through independently conducted studies that utilized multiple sourced agents and a variety of antigen-expressing target cell lines. However, the study has limitations, including the need to test additional tumor-targeting antibodies and ADCs to understand the magnitude of potential application that CA125 antagonists may have for cancers treated with antibody-based therapies, as well as the absence of *in vivo* data to corroborate the extensive *in vitro* results. Future research will broaden the evaluation of NAV-005 activity by including more regulatory agency-approved and experimental antibodies/ADCS that target CA125-expressing cancers. Furthermore, comprehensive *in vivo* studies are planned using optimized models with tumor xenografts that homogenously express CA125 levels across tumor cell lines when independently infused into mouse hosts, which will serve as a standard to evaluate NAV-005's effect on enhancing antibody and/or ADC efficacy against other CA125-expressing tumor xenografts. The development of these models are ongoing. The outcomes of these studies will be presented in a subsequent manuscript, aiming to further validate the current *in vitro* findings and to advance the development of high-affinity CA125 antagonists to counteract humoral immunosuppression mediated by CA125 in human studies.

Conclusion and Outlook

Conclusion The results of this study confirm the immunosuppressive impact of tumor-produced CA125 on anticancer therapeutic antibodies and ADCs. Moreover, our results indicate that a

CA125 antagonist such as NAV-005 could overcome CA125 immunosuppression and enhance the antitumor activity of therapeutic antibodies and ADCs in HIO-positive cancers.

Outlook CA125 is overexpressed in a number of cancers. While its negative impact on antibody-based therapy and clinical outcomes is still emerging, several independent studies have shown its immunosuppressive impact on antibody-mediated target cell killing (9,11,12,21,35,39). Therefore, agents capable of overcoming the immunosuppressive effects of CA125, such as NAV-005, may improve the efficacy of regulatory agency-approved antibody therapies like RTX in non-Hodgkin's lymphoma, potentially leading to better therapeutic outcomes in both newly diagnosed and relapsed patients (2,39). Moreover, while not evaluated in this study, the use of CA125 antagonists in HIO-positive cancers may improve not only the efficacy of therapeutic antibodies and ADCs but also the potential efficacy of patient-produced autoantibodies against dysregulated cancer cells (22-24).

Declarations

Authors have nothing to declare.

Abbreviations

HIO humoral Immuno-Oncology

ADCC antibody dependent cellular cytotoxicity

CDC complement dependent cellular cytotoxicity

ADC antibody drug conjugate

MBD mesothelin binding domain

SPR surface plasmon resonance

PBMC peripheral blood mononuclear cells

ELISA enzyme-linked immunosorbent assay

PTZ pertuzumab

RTX rituximab

FRA folate receptor alpha

MSLN mesothelin

v/v volume per volume

w/v weight per volume

Ethics approval and consent to participate

Not applicable

Consent for publication

Not applicable

Competing interests

The authors declare that they have no competing interests.

Funding

This study was funded by Navrogen.

Author contributions

Nicholas Nicolaides and Luigi Grasso conceived the idea and conceptualized the study. Nicholas Nicolaides, Luigi Grasso and J. Bradford Kline collected and analyzed the data. Nicholas Nicolaides, Luigi Grasso and J. Bradford Kline performed the statistical analysis of the data. Nicholas Nicolaides drafted the manuscript, and Luigi Grasso and J. Bradford Kline reviewed and edited the manuscript. All the authors read and approved the final draft.

Acknowledgements

The YOU-meso cell line was obtained from Dr. Raffit Hassan at the National Cancer Institute.

Data availability

All the data generated or analyzed during this study are included in this article. Further inquiries can be directed to the corresponding author.

References

1. Bast Jr RC, Xu FJ, Yu YH, Barnhill S, Zhang Z, Mills GB. CA125: The past and the future. *Int.* J Biol Markers. 1998;13(4):179-187.

2. Dilek I, Ayakta H, Demir C, Meral C, Ozturk M. CA125 levels in patients with non-Hodgkin lymphoma and other hematologic malignancies. Clin Lab Haematol. 2005;27(1):51-55.

3. Serreyn R, Deboever J, Martens G, Vandekerckhove D. Quantitative assessment of CA-125 in the normal ovary and in benign and malignant ovarian tumours. J Tumor Marker Oncol. 1991;5:341-49.

4. Meyer T and Rustin GJS. Role of tumour markers in monitoring epithelial ovarian cancer. British J Cancer. 2000;82(9):1535-1538.

5. Charkhchi P, Cybulski C, Gronwaldet J, et al. CA125 and ovarian cancer: A comprehensive review. Cancers. 2020;12(12):1-29.

6. Crombach G, Scharl A, Würz H. CA125 in normal tissues and carcinomas of the uterine cervix, endometrium and fallopian tube. II. Immunoradiometric determination in secretions, tissue extracts and serum. Arch Gynecol Obstet. 1989;244(2):113-122.

7. Beck EP, Moldenhauer A, Merkle E, et al. CA125 production and release by ovarian cancer cells in vitro. Int J Biological Markers. 1998;13(4):200-206.

8. Marth C, Zeimet AG, Widschwendter M, Daxenbichler G. Regulation of CA125 expression in cultured human carcinoma cells. Int J Biol Markers. 1998;13(4):207-209.

9. Grasso L, Kline JB, Nicolaides NC. Block-Removed Immunoglobulin Technology to enhance rituximab effector function by counteracting CA125-mediated immunosuppression Oncol Letters. 2022;23(1):1-10.

10. Pantankar M, Jing Y, Morrison JC, Belisle JA, Lattanzio FA, et al. Potent suppression of natural killer cell response mediated by the ovarian tumor marker CA125. Gyncol Oncol. 2005;99(3):704-713.

11. Kline JB, Kennedy RP, Albone E, Chao Q, Fernando S, et al. Tumor antigen CA125 suppresses antibody-dependent cellular cytotoxicity (ADCC) via direct antibody binding and suppressed Fc-γ receptor engagement Oncotarget. 2018;8(32):52045-52060.

12. Wang W, Somers EB, Ross EN, Kline JB, O'Shannessy DJ, et al. FCGR2A and FCGR3A genotypes correlate with farletuzumab response in patients with first-relapsed ovarian cancer exhibiting low CA125. Cytogenet Genome Res. 2017;152(4):169-179.

13. Kline JB, Fernando S, Ross EN, Grasso L, Nicolaides NC. Tumor-shed antigen CA125 blocks complement-mediated killing via suppression of C1q-antibody binding. Eur J Immunol. 2018;48(11):1872-1882.

14. DiLillo DJ, Ravtech JV. Fc-receptor interactions regulate both cytotoxic and immunomodulatory therapeutic antibody effector functions. Cancer Immunol Res. 2015;3(7):704-713.

15. Zhou X, Hu W, Qin X. The role of complement in the mechanism of action of rituximab for B-cell lymphoma: implications for therapy. Oncologist. 2008;13(9):954-966.

16. Ruck T, Bittner S, Wiendl H, Meuth SG. Alemtuzumab in multiple sclerosis: mechanism of action and beyond. Int J Mol Sci. 2015;16(7):16414-16439.

17. Mandó P, Rivero SG, Rizzo MM, Pinkasz M, Levy EM. Targeting ADCC: A different approach to HER2 breast cancer in the immunotherapy era. Breast. 2021;60:15-25.

18. Spiridon CI, Ghetie MA, Uhr J, Marches R, Li JL, Shen GL, Vitetta ES. Targeting multiple HER-2 epitopes with monoclonal antibodies results in improved antigrowth activity of a human breast cancer cell line *in vitro* and *in vivo*. Clin Cancer Res. 2002;8(6):1720-1730.

19. Hsu YF, Ajona D, Corrales L, Lopez-Picazo JM, Gurpide A, et al. Complement activation mediates cetuximab inhibition of non-small cell lung cancer tumor growth *in vivo*. Mol Cancer. 2010;9:139-147.

20. Casneuf T, Xu XS, Adams HC, Axel AE, Chiu C, et al. Effects of daratumumab on natural killer cells and impact on clinical outcomes in relapsed or refractory multiple myeloma. Blood Adv. 2017;1(23):2105-2114.

21. Vergote I, Armstrong D, Scambia G, Teneriello M, Sehouli J, et al. A randomized, double-blind, placebo-controlled, phase III study to assess efficacy and safety of weekly farletuzumab in combination with carboplatin and taxane in patients with ovarian cancer in first platinum-sensitive relapse. J Clin Oncol. 2016;34(19):2271-2278.

22. Staff C, Magnusson CGM, Hojjat-Farsangi M, Mosolits S, Liljefors M, et al. Induction of IgM, IgA and IgE antibodies in colorectal cancer patients vaccinated with a recombinant CEA protein. J Clin Immunol. 2012;32(4):855-865.

23. Brändlein S, Pohle T, Ruoff N, Wozniak E, Müller-Hermelink HK, Vollmers HP. Natural IgM antibodies and immunosurveillance mechanisms against epithelial cancer cells in humans. Cancer Res. 2003;63(22):7995-8005.

24. Mazor RD, Nachum N, Gilboa A, Stoler-Barak L, Moss L, et al. Tumor-reactive antibodies evolve from non-binding and autoreactive precursors. Cell. 2022;185:1208-1222.

25. Chen SH, Hung WC, Wang P, Paul C, Konstantopoulos K. Mesothelin binding to CA125/MUC16 promotes pancreatic cancer cell motility and invasion via MMP-7 activation. Scientific Reports 2013;3(1870):1-10.

26. Xiang X, Feng M, Felder M, Connor JP, Man YG, et al. HN125: A novel immunoadhesin targeting MUC16 with potential for cancer therapy. J Cancer. 2011;2:280-291.

27. Nicolaides NC, Kline JB, Grasso L. NAV-001, a high-efficacy antibody-drug conjugate targeting mesothelin with improved delivery of a potent payload by counteracting MUC16/CA125 inhibitory effects. PLoS One 2023;18(5):e0285161.

28. Nadcarni DV. Conjugations to endogenous cysteine residues. Methods Mol Biol. 2020;2078:37-49.

29. Kaneko O, Gong L, Zhang J, Hansen JK, Hassan R, et al. A binding domain on mesothelin for CA125/MUC16. J Biol Chem. 2009;284(6):3739-3749.

30. Li F, Emmerton KK, Jonas M, Zhang X, Miyamoto JB, Setter JR, et al. Intracellular released payload influences potency and bystander-killing effects of antibody-drug conjugates in preclinical models. Cancer Res. 2016;76(9):2710-2719.

31. Kline JB, Grasso L, Nicolaides NC. ICAM-1 is over-expressed by cancers and negatively impacts antibody-based therapies including antibody-drug conjugates. Eur J Immunol. 2025;55:e202451611.

32. Gupta A, Michelini F, Shao H, Yeh C, Drago JZ, et al. EGFR-directed antibodies promote HER2 ADC internalization and efficacy. Cell Reports Med. 2024;5:1-11.

33. Hassan R, Ebel W, Routhier EL, Patel R, Kline JB, et al. Preclinical evaluation of MORAb-009, a chimeric antibody targeting tumor-associated mesothelin. Cancer Immunol. 2007;7(19):20-30.

34. Hassan R, Schweizer C, Lu KF, Schuler B, Remaley AT, Weil SC, Pastan I. Inhibition of mesothelin-CA125 interaction in patients with mesothelioma by the anti-mesothelin monoclonal antibody MORAb-009: implications for cancer therapy. Lung Cancer. 2010;68(3):455-459.

35. Nicolaides NC, Schweizer C, Wang W, Somers EB, Ross EN, et al. CA125 suppresses immune-effector function of amatuximab and elevated levels are associated with reduced amatuximab clinical response in first line mesothelioma patients. Cancer Biol Ther. 2018;19(7):622-630.

36. Coënon1 L, Villalba M. From CD16a biology to antibody dependent cell-mediated cytotoxicity improvement. Front Immunol. 2022;13:913215.

37. Gogesch P, Dudek S, van Zandbergen G, Waibler Z, Anzaghe M. The role of Fc receptors on the effectiveness of therapeutic monoclonal antibodies. Int J Mol Sci. 2021;22(16):8947.

38. Rupert PB, Buerger M, Friend DJ, Strong RK. Structural elucidation of the mesothelin-mucin-16/CA125 interaction. Structure. 2024;32:1049–1054.

39. Procházka V, Faber E, Raida L, Kapitáňová Z, Langová K, Indrák K, Papajík T. High serum carbohydrate antigen-125 (CA-125) level predicts poor outcome in patients with follicular lymphoma independently of the FLIPI score. Int J Hematol. 2012;96(1):58-64.

40. Charkhchi P, Cybulski C, Gronwald J, Wong FO, Narod SA, Akbari MR. CA125 and ovarian cancer: A comprehensive review. Cancers. 2020;12(12):3730-3759.

41. Fang C, Cao Y, Liu X, Zeng XT, Li Y. Serum CA125 is a predictive marker for breast cancer outcomes and correlates with molecular subtypes. Oncotarget. 2017;8(38):63963-63970.

42. Streppel MM, Vincent A, Mukherjee R, Campbell NR, Chen SH, et al. Mucin 16 (cancer antigen 125) expression in human tissues and cell lines and correlation with clinical outcome in adenocarcinomas of the pancreas, esophagus, stomach, and colon. Hum Pathol. 2012;43(10):1755-1763.

43. Grasso L, Kline JB, Nicolaides, NC. Bypassing the immunosuppressive effects of CA125/MUC16 via re-engineered rituximab (NAV-006) to improve its antitumor activity *in vivo*. Antibody Ther 2025;8:171-176.

44. Li C, Zhang C, Li Z, Samineni D, Lu D, et al. Clinical pharmacology of vc-MMAE antibody–drug conjugates in cancer patients: learning from eight first-in-human Phase 1 studies. MABS. 2019;12(1):e1699768, 1-12.

45. de Zwart M, Lausecker B, Globig S, Neddermann D, Le Bras B, et al. Co-Medication and interference testing in bioanalysis: A European bioanalysis forum recommendation. Bioanalysis. 2016;8(19):2065-2070.

Figure legends

Figure 1. MBD1-Fc binds to CA125 but does not prevent CA125 inhibition of antibody-CD16a binding. (A) Testing for MBD1-Fc binding to full length CA125 and recombinant N- (CA125-N) and C- (CA125-C) terminal CA125 fragments. Significance was observed for binding to CA125 and CA125-C as compared to HSA control ($P < 0.0001$). (B) Testing for MBD1-Fc antagonism on CA125 to enhance RTX-CD16a binding. MBD1-Fc could not overcome CA125 suppression on RTX-CD16a binding as compared to no treatment ($P < 0.01$). Statistical analysis was determined using the Student's t test.

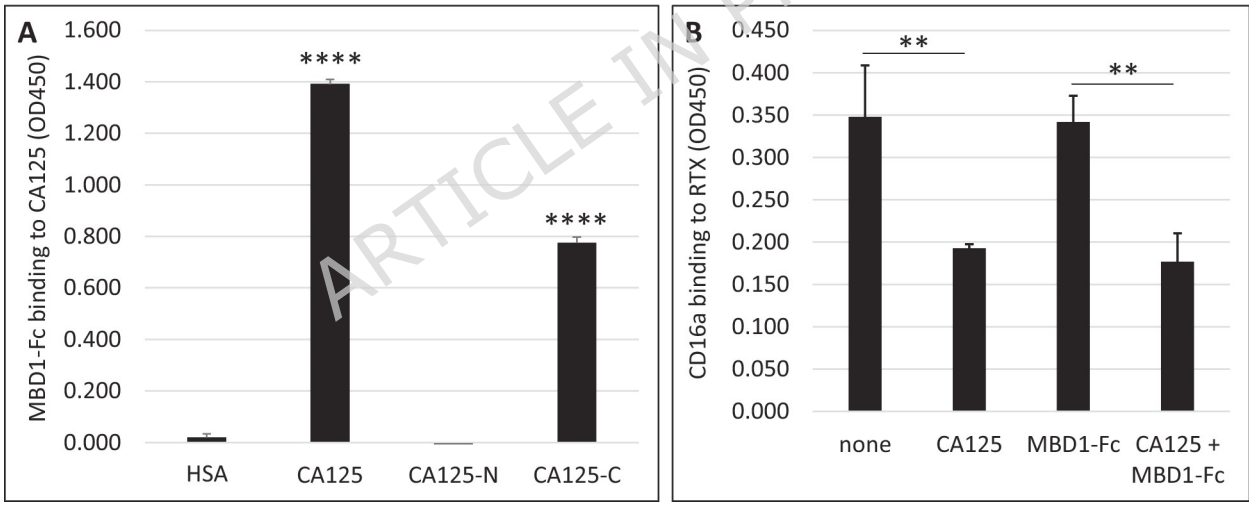

Figure 2. MDB-Fc fusion proteins with multiple MBDs are robust CA125 antagonists. (A) Schematic of MBD-Fc fusion proteins containing one, two, or three MBDs linked by a GGGGS amino acid spacer (in red) fused to the human IgG1 Fc domain. All three fusion proteins contain the hinge region within the Fc domain and are homodimers. (B) MBD-Fc fusion proteins significantly bind CA125 but not the HSA negative control ($P < 0.001$). CA125 binding to RTX significantly suppresses RTX-CD16a (C) and RTX-C1q (D) engagement which is abrogated by MBD2-Fc and MBD3-Fc fusion proteins but not MBD1-Fc ($P < 0.0001$). Statistical analysis was determined using ANOVA.

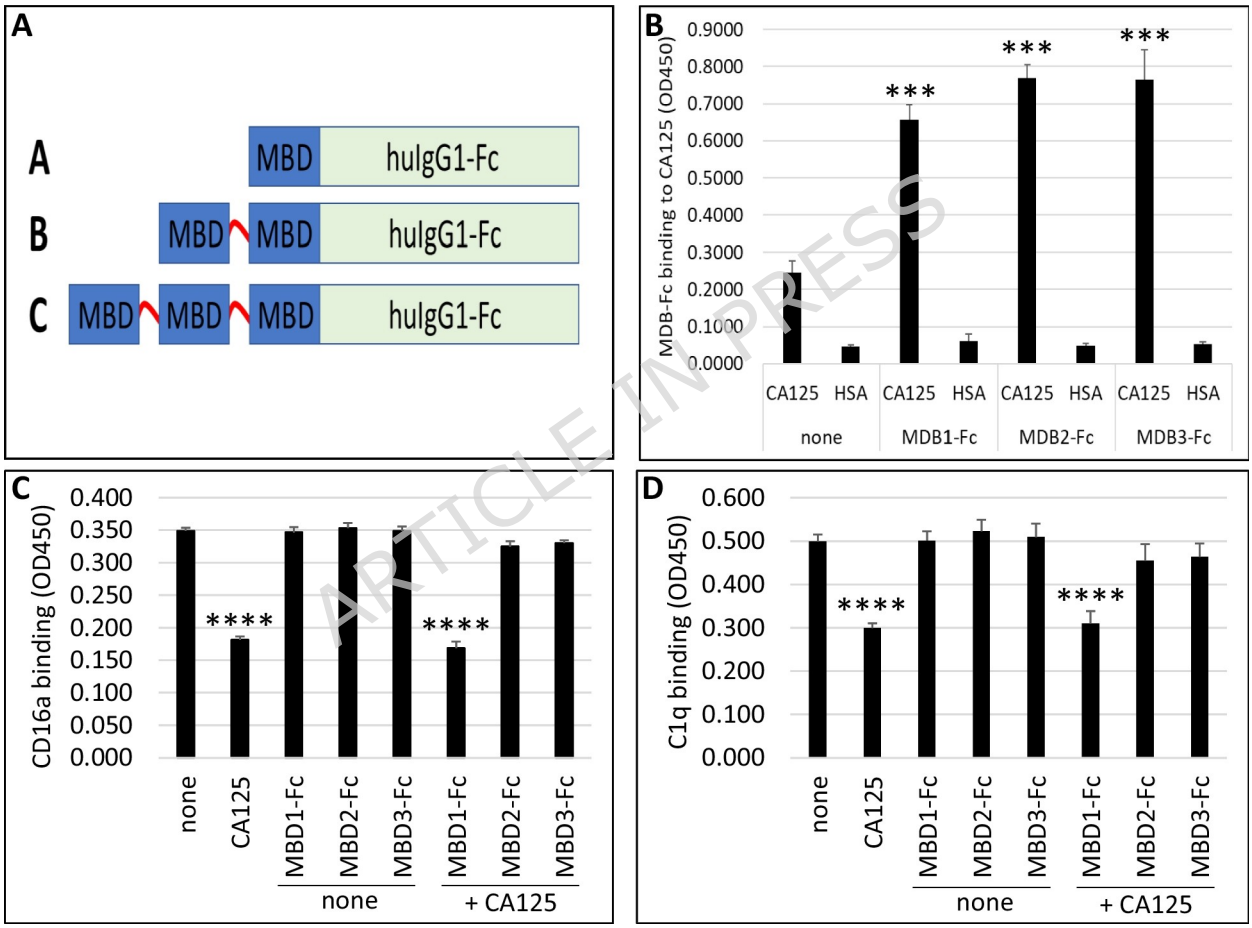

Figure 3. Binding affinity of MBD-Fc proteins containing one (MBD1-Fc) or two (MBD2-Fc) MBD motifs to CA125. Surface plasmon resonance was used to calculate the binding affinities for MBD1-Fc (K_D = 65 pM) and MBD2-Fc (K_D = 15 pM).

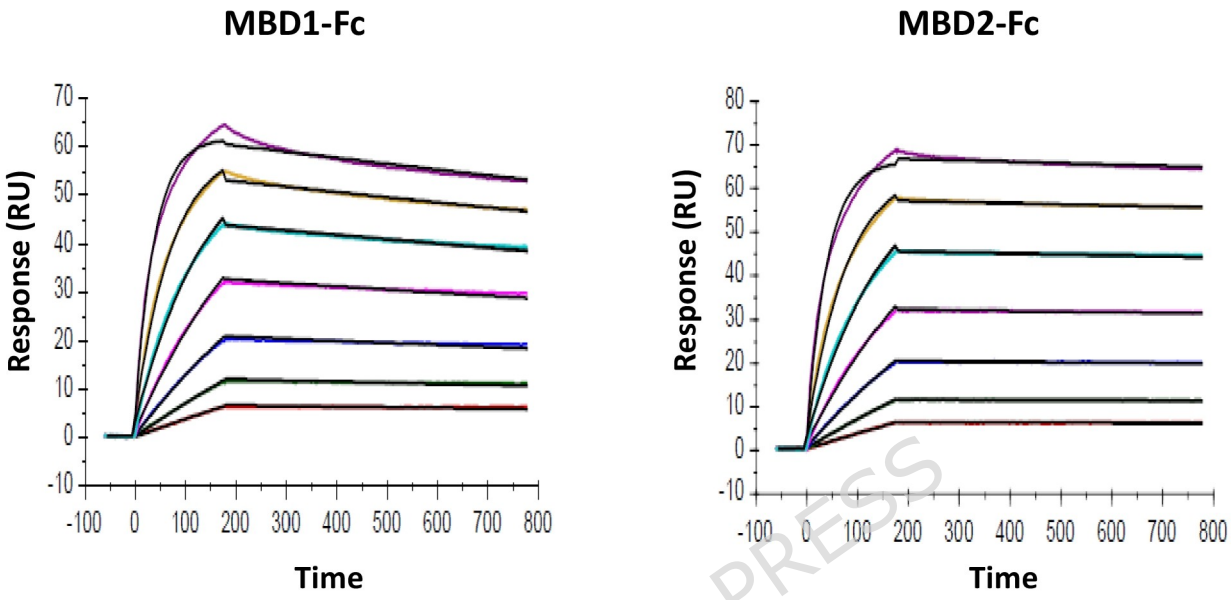

	Analyte	Ka (1/Ms)	Kd (1/s)	KD (M)	Rmax (RU)	Chi² (RU²)
MBD1-Fc	rCA125/MUC16	3.32E+06	2.16E-04	6.52E-11	61.29	0.323
MBD2-Fc	rCA125/MUC16	3.17E+06	4.72E-05	1.49E-11	67.37	0.244

Figure 4. MBD-Fc fusion proteins containing two MBD motifs abrogate CA125 immunosuppression of antibody-mediated CD16a activation and CDC. CD16a activation and CDC killing effects of antibody in the presence of CA125 was tested alone or in the presence of MBD-Fc proteins. (A) MBD2-Fc but not MBD1-Fc is able to overcome suppressed Jurkat-CD16a activation by NAV-007 against OVCAR3 cells in the presence of CA125 ($P < 0.0001$).

MBD-Fc fusion proteins alone had no effect CD16a activation. The percentage of enhanced CD16a activation was calculated as ((NAV-007+CA125+MBD-Fc lumens / NAV-007+CA125 lumens)-1) × 100. (B) MBD2-Fc but not MBD1-Fc fusion protein is able to overcome suppressed RTX-mediated CDC against Daudi cells in the presence of CA125 ($P < 0.0001$). The percentage of enhanced CDC was calculated as (1-(RTX+CA125+MBD-Fc+complement lumens / RTX+CA125+ complement lumens)) × 100. Statistical analysis was determined using ANOVA.

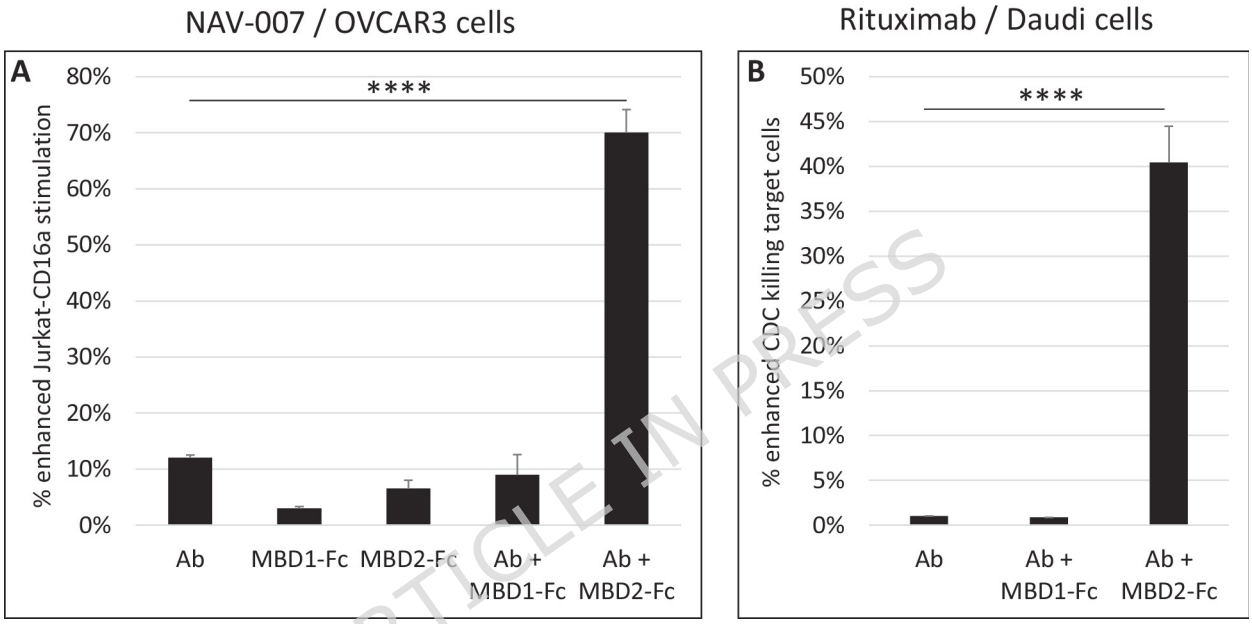

Figure 5. MBD2-Fc fusion protein abrogates the immunosuppressive effects of membrane-bound CA125 on ADCC. (A) Testing the ADCC effects of human PBMCs by MBD1-Fc, MBD2-Fc, RTX and PTZ on $CA125^{+}/HER2^{+}/CD20^{+}$ OVCAR-CD20 cells. PTZ and RTX alone elicit ADCC target cell killing ($P < 0.0001$) in contrast to either MBD-Fc fusion protein alone. (B) MBD2-Fc fusion protein significantly enhances the ADCC activity of PTZ and RTX against OVCAR-CD20 cells in contrast to MBD1-Fc ($P < 0.0001$). The percentage of ADCC killing (A) and enhanced ADCC activity (B) were calculated as (1-(Ab+PBMC lumens / PBMC lumens)) × 100 and 1-(Ab+MBD-Fc+PBMC lumens / Ab+PBMC lumens), respectively. Panel C shows the purity and stability of each fusion protein via non-denaturing SDS-PAGE analysis. Statistical analysis was determined using ANOVA.

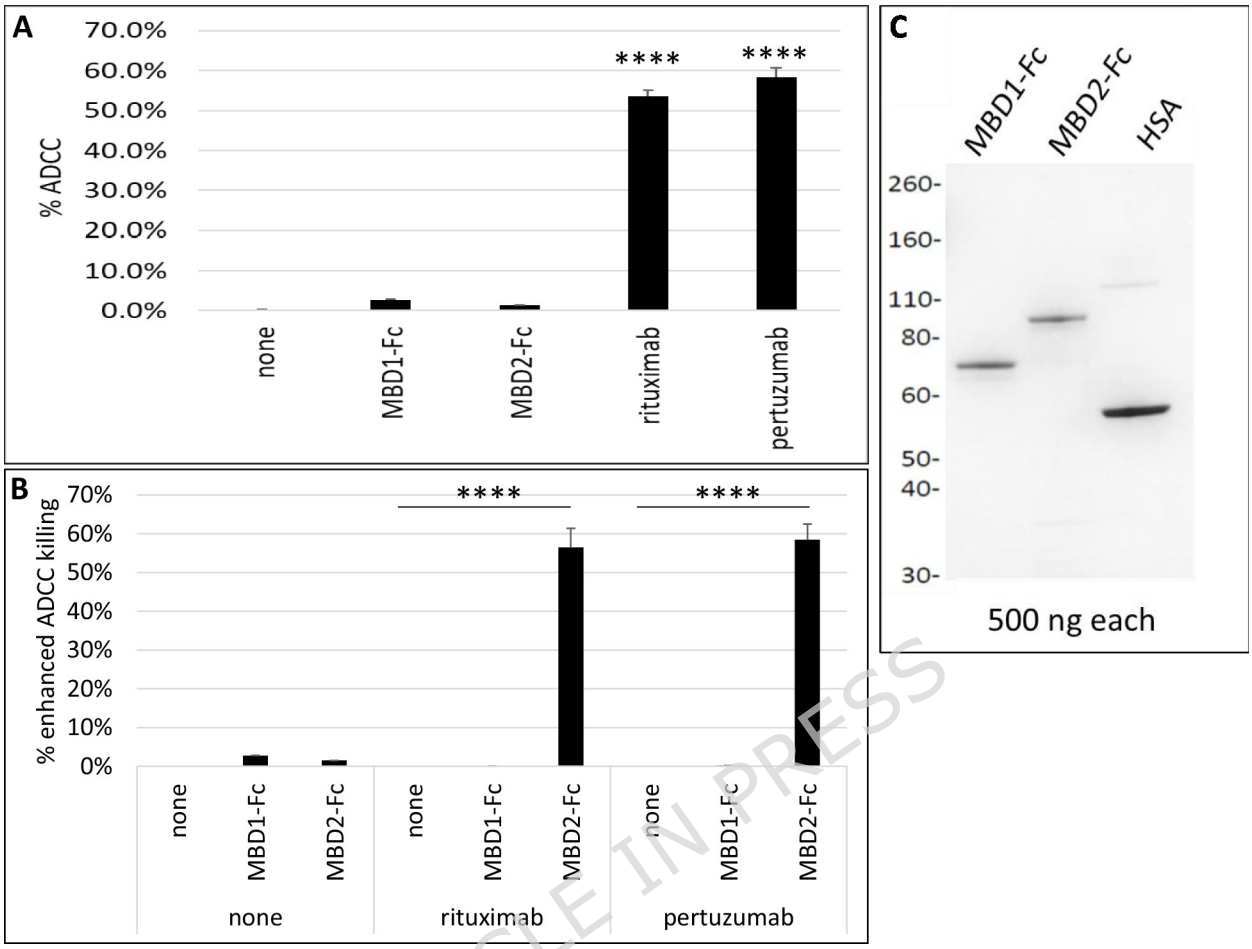

Figure 6. MBD2-Fc enhances ADC cytotoxicity against CA125-expressing target cells. MBD2-Fc fusion protein enhances the cytotoxicity of the anti-MSLN SS1-SN38 ADC against CA125^{+}/MSLN^{+} SW1990, YOU-meso, and OVCAR3 cell lines ($P < 0.01$). SS1-SN38 ADC has enhanced cytotoxicity against the isogenic CA125^{-}/MSLN^{+} OVCAR-KD1 cell line as compared to parental OVCAR3 cells ($P < 0.01$). MBD2-Fc does not enhance SS1-SN38 ADC cytotoxicity

against the CA125$^-$ OVCAR-KD1 cell line. The red numbers in each column are the IC_{50} (ng/mL) for SS1-SN38 ADC on each cell line alone. The percentage of ADC cytotoxicity was calculated via the formula (1-(treated cells / untreated cells)) × 100, and the experiments were performed in triplicate. Statistical significance was calculated via Student's t test comparing each cell line treated with ADC vs ADC + MDB2-Fc. Statistical analysis was determined using the Student's t test.

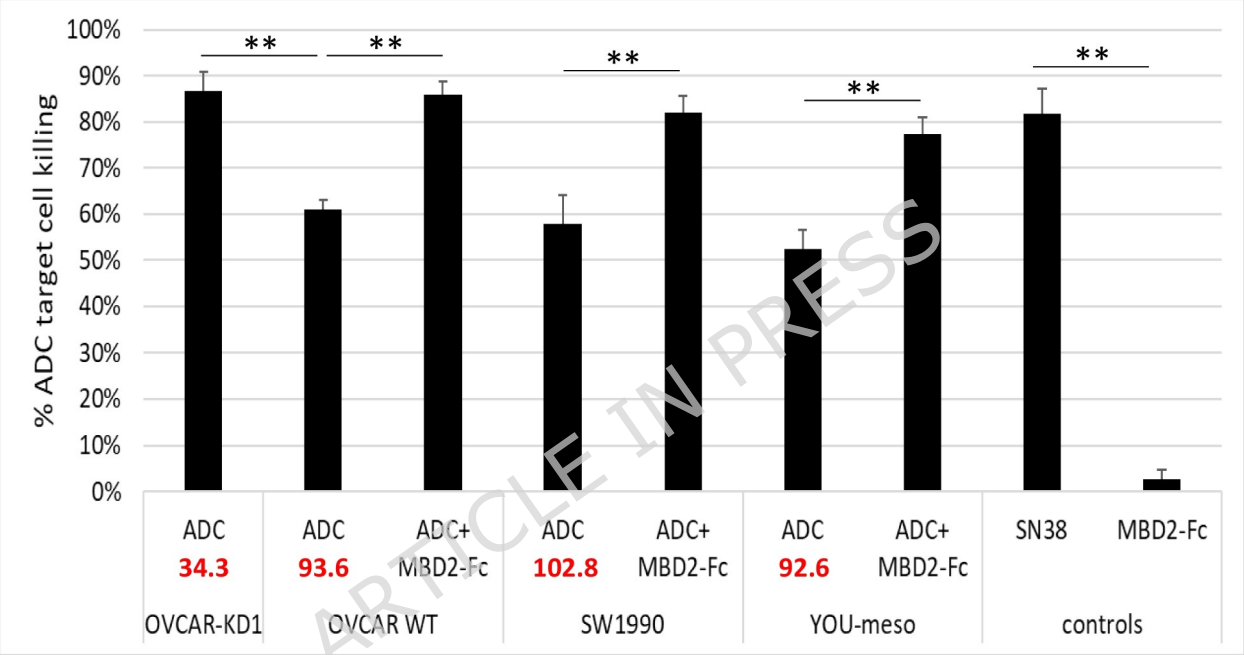

Figure 7. Cell surface CA125 expression reduces ADC internalization. The SS1 and RTX antibodies were pHrodo labeled and assayed for internalization using CA125$^+$/MSLN$^+$ expressing OVCAR3 and its isogenic CA125$^-$/MSLN$^+$ OVCAR-KD1 cells. Antibody internalization was measured from 1 minute to 24 hours +/- MBD2-Fc. RTX served as a negative control to monitor nonspecific uptake. Panel A, OVCAR-KD1 cells (blue line) had significant uptake of SS1 as compared to OVCAR3 parental cells (29% enhanced uptake at 1 hour). MBD2-Fc fusion protein significantly enhances SS1 internalization in OVCAR3 (black line) ($P < 0.01$) but not CA125-null OVCAR-KD1 cells (blue vs red lines). Percent enhanced internalization is calculated by comparing SS1 uptake in OVCAR3 vs. other conditions. Panel B shows a schematic diagram of the potential mechanism by which MBD2-Fc (NAV-005) enhances

antibody internalization and improves ADC target cell killing by liberating the ADC from membrane-bound CA125. Statistical analysis was determined using the Student's t test.